Model-Based Control of a Hydronic Radiant Slab for Peak Load Reduction

Vasken Dermardiros[1], Charalampos Vallianos[1], Andreas K. Athienitis[1], Scott Bucking[2]
[1]Concordia University, Montreal, QC, Canada
[2]Carleton University, Ottawa, ON, Canada

Abstract

This paper presents a model and model-based predictive control (MPC) methodology for a hydronic radiant slab system for an archetype zone that allows deep daylight penetration and cross ventilation. The methodology is applied to a cold-climate case study, the Varennes library, located near Montreal, Quebec (Canada's first institutional net-zero energy building). We used an implicit finite difference based approach to model the heat transfer in the room and slab. The work presented lays the groundwork for the future implementation of MPC into the library and for archetype-based studies for controls.

Conventionally, hydronic radiant slabs are controlled through inlet-oulet temperature differentials and based on ambient conditions correlations. Predictive measures are seldom applied which can be beneficial for peak demand reduction and shifting. The MPC algorithm here replicates a pre-cooling strategy in anticipation of mid-day solar gains. However, the effectiveness of the hydronic slab is greatly influenced by its covering favouring low thermal resistance. The methodology can be extended for other storage mediums and fine-tuned for the specific cost and performance needs of the project.

Introduction

Net-Zero Energy (NZE) buildings are complex and yet all their systems have to function harmoniously in order to achieve their net-zero target (Bucking et al., 2014). Poor operational practices (such as using incorrect outside air and thermostat settings) and unaccounted occupant behaviour could combine to increase energy use by up to 50-60% more than necessary (NBI, 2013). The challenges can be addressed during the design and operation stages of a building.

Model predictive control (MPC) – or receding horizon control – refers to a class of control algorithms that utilize a model of a system and forecasts to predict and optimize the system's future response (Candanedo et al., 2015; Lee, 2011; Qin and Badgwell, 2003; Camacho and Bordons, 2007). The control variables are optimized to minimize the cost function over a prediction horizon. However, only the first or first few control sequences are applied. For example, the controller can be set to minimize energy use over a period or to minimize the peak power required. The underlying models can be based on heat transfer equations solved using a finite difference approach (as per this paper) or trained using collected data. Both types should be refined over time upon the availability of newer data.

Temporal mismatch between source availability and requirement can be mitigated via thermal and electrical storage systems. When electricity or heat is available but not needed, storage systems are necessary to harness and retain the energy until a future need. Here, we focus on a hydronic radiant concrete slab thermal energy storage (TES) system. Hydronic radiant floor systems offer many advantages and through proper design and control can reduce and shift the thermal load of a building and minimize temperature fluctuations (Chen et al., 2012). Radiant systems circulate water with temperatures closer to the zone temperature and thus can utilize condenser-side heat recovery from air or ground source heat pumps at higher efficiencies (Olesen, 2008). Free cooling, heat recovery, condensing boilers, building-integrated photovoltaic and thermal (BIPV/T) systems are other options of inexpensive or recovered heat that can be utilized in radiant slabs. Or simply having the ability to operate the HVAC plant during off-peak periods to pre-heat or pre-cool the slab in preparation of a future load.

In current practice, hydronic radiant slabs are controlled through inlet-oulet temperature differentials (typically in 5 to 10K range) and based on ambient conditions (Nall, 2013). The slab acts as a thermal buffer and either releases or captures heat depending on the room temperature; there is a self-regulating effect. Predictive measures are seldom applied which can be beneficial for peak reduction and shifting by preemptively pre-heating or cooling the slab in anticipation of a future load.

Model-based controls were applied in the oil and petrochemical industries as early as the 1950s (Lee, 2011; Qin and Badgwell, 2003). The earliest noted application for MPC as supervisory control for a

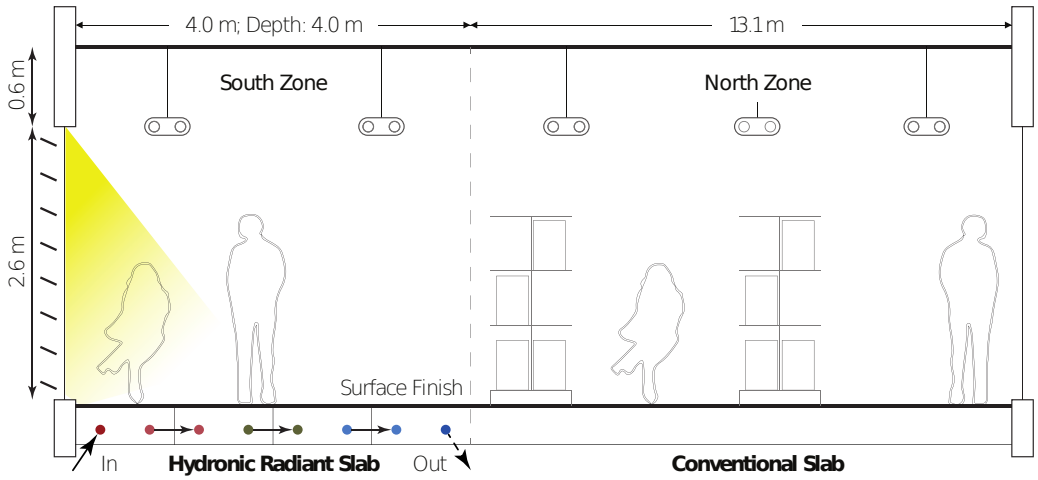

Figure 1: Library cross-section.

Figure 2: Library photos. [1] Exterior, [2] Second floor, [3] Second floor, looking towards South windows. (A) 120 kW PV array, (B) Passive shading device, (C) Displacement ventilation integrated to stacks, (D) Hydronic radiant slab, (E) Underfloor displacement ventilation diffuser. For brevity, only features relevant to this study are shown.

building was from 1988 (Coffey et al., 2010) . However, due to computational requirements and financially unjustifiable rate of returns, it did not receive much attention until the 2000s. The Swiss Opti-Control Team (Oldewurtel et al., 2010, 2012), May-Ostendorp, Henze *et al.* from Colorado U (2011), O'Brien, Gunay from Carleton U *et al.* (2014), to name a few, have worked extensively on MPC applied to buildings using varied approaches.

MPC is a mature technology in the process industry. However, it is still sparsely applied in the building industry and it is difficult to obtain real-world performance data. The work presented in this paper lays the groundwork for the future implementation of MPC into the library. Figure 2 shows images of the library's exterior and 2nd floor interior.

The optimization routines in this paper rely on simplified models of the room and slab. Simplified models are conducive for controls. They are simpler to calibrate using measured data, run quicker and can be troubleshooted with greater ease. Finally, the models must be designed to give accurate enough predictions to drive control decisions. (Candanedo and Athienitis, 2011; Wang and Ma, 2008; Hovgaard et al., 2013)

Method

The body of the paper is divided into 3 sections: (1) library section and slab model description, (2) model-based controls, and (3) effect of design on control.

Room and Slab Model Description

The section shown in Figure 1 represents a slice of the library oriented North-South; it is also shown in Figure2-B. The section serves as an archetype zone of an institutional building that allows deep daylight penetration and cross ventilation through the use of motorized windows on both sides. The U.S. National Renewable Energy Laboratory's Research Support Facility (NREL RSF) features a similar concept.

The library section is divided in two parts: north and south zones. The South's dimensions are 4 m

$$\begin{bmatrix} \sum_j^N U_{1j} + \sum_k^M U_{1k} + \frac{C_1}{\Delta t} & -U_{12} & \dots & -U_{1N} \\ \vdots & \vdots & \ddots & \vdots \\ -U_{N1} & -U_{N2} & \dots & \sum_j^N U_{Nj} + \sum_k^M U_{Nk} + \frac{C_N}{\Delta t} \end{bmatrix} \begin{Bmatrix} T_1 \\ \vdots \\ T_N \end{Bmatrix}^{t+1} = \begin{Bmatrix} \dot{Q}_1 + \sum_k^M (U_{1k} T_k) + \frac{C_1}{\Delta t} T_1^t \\ \vdots \\ \dot{Q}_N + \sum_k^M (U_{Nk} T_k) + \frac{C_N}{\Delta t} T_N^t \end{Bmatrix} \quad (1)$$

by 4 m by 3.2 m in height and has a 2.6 m triple-glazed low-emissivity coated window (80% window-to-wall ratio). The window is partially shaded by fixed exterior louvers 165 mm wide, tilted 20°, spaced at 250 mm and installed 100 mm from the glass. The louvers make it so that the slab surface scarcely receives beam radiation, *i.e.* solar patches do not occur. The concrete slab is 75 mm in depth. The pipes for the hydronic system are placed at the bottom of the slab and spaced 250 mm apart on-center in a serpentine pattern. The water flowrate in the library is variable, however in this paper we have it constant with varying temperature. The slab is finished with pale vinyl tiles. The North's dimensions are 13.1 m by 4 m by 3.2 m in height and has the same type windows but cover 10% of the gross wall area (10% window-to-wall ratio). The slab on the north side does not have pipes.

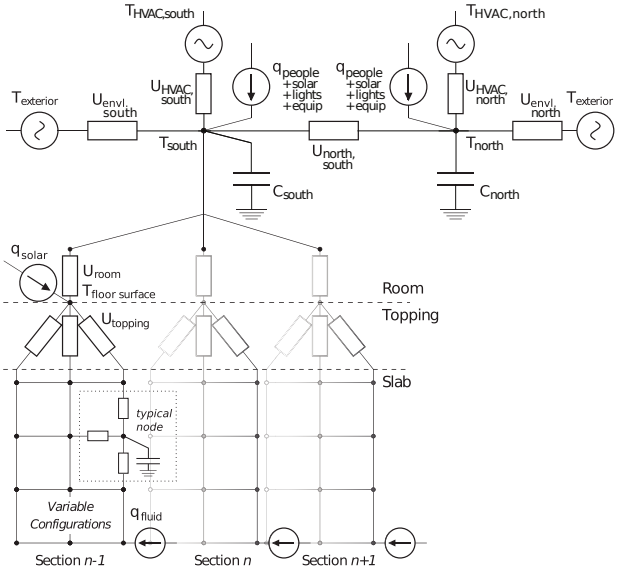

*Figure 3: Circuit representation of library section, surface finish and slab. Each zone is represented by a single node with a single capacitance representing the effective thermal mass of the walls and furniture. It is connected to the exterior ambient air via an effective windowed wall conductance. The slab is separated in 4 sections. Each section is represented by a 5*4 (width*depth) 2-D grid. All the nodes have a capacitance representing the concrete volume and are connected to one another. The side and bottom boundary of the slab are adiabatic. The heat input from the fluid flow is connected to the bottom corner. The slab top nodes are connected by conductors representing the topping material and merge into the slab section's floor surface node. The floor surface receives part of the solar gains passing through the window and connect to the zone air node through a combined convective and radiative conductance. The north zone does not have an active slab. Best viewed on a digital copy.*

For the simulation, Montreal weather is used since it is the closest major city to Varennes. Occupancy and internal loads are assumed to be present when the library is open. A 7.53 W/m^2 lighting power density and 5.4 W/m^2 for equipment are used. The heating/cooling setpoints are $21/26°C$ when occupied (9:00AM to 9:00PM) and $17/30°C$ when unoccupied. Three sunny cold winter days are presented and used in the analysis (see Figure 4 for the imposed weather conditions and internal gains). The full simulation is ran for 5 days; the first day is used for initialization; the 5^{th} day is used as padding to finish the optimization on day 4; only the middle 3 days are shown. In a future work, whole year simulations will be performed. The space directly below the one considered is equally conditioned and the floor is well insulated. For this study, the boundary condition below the radiant slab is considered adiabatic. Detailed solar calculations are done to determine the proportion of solar radiation coming through the window onto the slab sections and the rest of the room. All other simulation parameters and material properties are summarized in Table 2 presented at the end of this paper.

Models are used to drive decisions (Candanedo et al., 2011; Hovgaard et al., 2013). For model based controls, simpler models are often preferred since they have fewer parameters that need to be determined. Computationally, they can be used efficiently. An implicit 1st-order approximation of Fourier's Law of Heat Conduction is used to model the thermal behaviour of the room and slab (Dermardiros, 2015, see Section A.1) as shown in the following equation:

$$\sum_j [U_{ij}^{t+1}(T_j^{t+1} - T_i^{t+1})] + \sum_k [U_{ik}^{t+1}(T_k^{t+1} - T_i^{t+1})] - \frac{C}{\Delta t}(T_i^{t+1} - T_i^t) + \dot{Q}_i^{t+1} = 0 \quad (2)$$

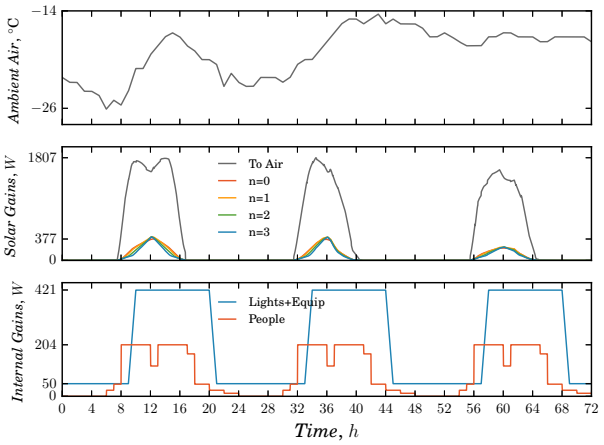

Figure 4: Weather inputs and internal gains. In the second chart, $n = \{0, 1, 2, 3\}$ represent the 4 equal south floor surfaces receiving solar gains starting from near the window to further inside. Internal gains for the north side are scaled proportionally to its area.

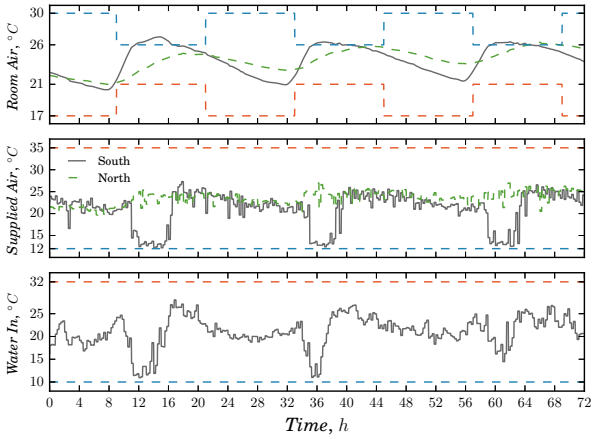

Figure 5: MPC result for a 75 mm deep tile-covered slab. Best viewed on a digital copy.

And generalized into a matrix form in Equation (1). The nomenclature used in this paper is listed at the end in Table 3.

The zones themselves are modelled with single conductances representing the influence of the exterior conditions and with single capacitances representing the effective thermal storage effect of the walls, air and furniture in the space. The HVAC system is modelled as a simple constant air volume system where the HVAC system is a node and is connected to the zone air node with conductance:

$$U_{\text{HVAC,Zone}} = \text{ACH} \cdot \forbar{V} \cdot \rho_{\text{air}} \cdot c_{\text{p,air}} \cdot 3600^{-1} \qquad (3)$$

The southern slab containing the piping is discretized in smaller parts. First, the slab surface is partitioned into a few sections (4 slab sections of 4 m^2 are used in this paper). The sections are discretized into 2-dimensional volumes: 5 nodes in width and 4 in depth. The concrete depth is 75 mm for the base scenario. Along the direction of fluid flow, the temperatures are assumed constant within a node of a section. The fluid exiting a section after having transferred energy to the slab enters the following section. The analogous electrical circuit equivalent of the thermal network is shown and explained in Figure 3. The temperature of the fluid travelling through a slab section follows an exponential regime (Cengel et al., 2011, see Ch.8). The net transfer units (NTU) equation and resulting outlet water temperature are shown:

$$NTU = \frac{h_{\text{conv+cond}}\ A_{\text{wetted}}}{\dot{m}_{\text{fluid}}\ c_{\text{p,fluid}}}$$

$$T^{t+1}_{\text{W,out},n} = T^{t+1}_{\text{W,in},n}\ e^{-NTU} + T^{t+1}_{\text{wetted}}\left(1 - e^{-NTU}\right) \qquad (4)$$

The wetted area represents the pipe surface area in contact with the water. The pipe's surface temperature is given by the concrete slab node onto which the source is connected. The water outlet of a given slab section becomes the inlet of the following:

$$T_{\text{W,out},n} = T_{\text{W,in},n+1}, \quad n \in [1, \textit{slab sections}] \qquad (5)$$

Given the inlet and outlet temperatures, the amount of heat injected or removed into the slab can be determined:

$$\dot{Q}^{t+1}_{W,n} = \dot{m} \cdot c_p \cdot \left(T^{t+1}_{\text{W,out},n} - T^{t+1}_{\text{W,in},n}\right)\Big|_{\text{fluid}} \qquad (6)$$

The water flow rate and HVAC air flow rate are kept constant. Fan and pump power are not considered. The library space is open and air is allowed to flow between the north and south zones.

Model-Based Controls

The model-based predictive control (MPC) scheme will maintain the setpoint profile by employing future predictions of the weather and attempt to minimize a predefined cost function. For this study, the future predictions are deterministic, however stochastic and uncertainty-based predictions are planned for a future work. The cost function can vary from project to project. Since the space is part of a library, the cost function penalizes times when the room temperature is outside the setpoint boundaries and penalizes

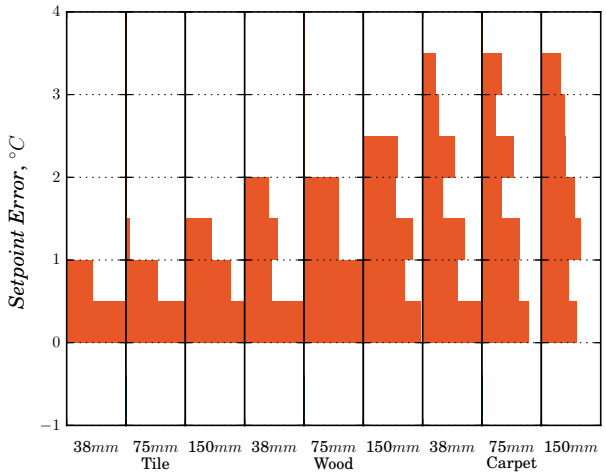

*Figure 6: Number of minutes when **south** room temperature is outside the setpoints for the 3 days simulated. Values are for the various finishes and for three concrete thicknesses. Positive (red) values signify overheating. The x-direction of the plot is limited to 300 minutes. Setpoint errors just below or above 0 are more frequent but tolerable. The vertical axis is divided in 0.5°C increments.*

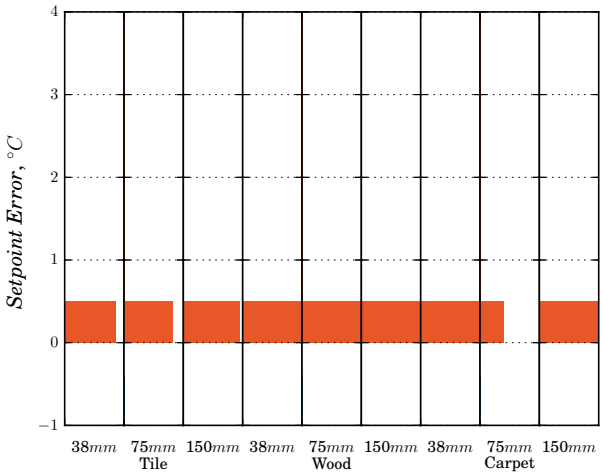

*Figure 7: Number of minutes when **north** room temperature is outside the setpoints for the 3 days simulated. Values are for the various finishes and for three concrete thicknesses. Positive (red) values signify overheating. The x-direction of the plot is limited to 300 minutes. Setpoint errors just below or above 0 are more frequent but tolerable. The vertical axis is divided in 0.5°C increments.*

when the system uses excessive electrical power and energy which are either larger than the installed capacity or exact a heavy utility bill. The optimization is performed on the library section. A cooling load is analogous of a need to extract and remove heat. On the building level, in winter, south facing and core zones often require cooling whereas the other zones require heating. The heat from the south zones is removed and transferred to the adjacent zones. If the heating demand of the adjacent zones is not satisfied, only then would auxiliary heat be used.

There are three control variables: the north and south air and water temperatures. They are optimized over the longer (8 hour) prediction horizon, but only the control sequences within the shorter (1 hour) control horizon are applied. Once the control horizon trajectory is applied, the process is repeated. For the following iteration, the control sequences past the control horizon – that were optimized for but not applied – serve as a warm start for the optimization. There are 16 temporal steps in the prediction horizon per control variable (48 dimensional problem). The cost function is central to MPC strategies and is defined:

$$\begin{aligned} \text{minimize} \quad & C_{\text{SP}} + C_{\text{ROC,W}} + C_{\text{ROC,A}} + \\ & C_{\text{PH,A}} + C_{\text{E}} \\ \text{subject to} \quad & T_{\text{W,min}} \leq T_{\text{W,in,0}} \leq T_{\text{W,max}} \\ & T_{\text{A,min}} \leq T_{\text{A}} \leq T_{\text{A,max}}\big|_{\text{south}} \\ & T_{\text{A,min}} \leq T_{\text{A}} \leq T_{\text{A,max}}\big|_{\text{north}} \end{aligned} \tag{7}$$

The largest weight is given to the setpoint cost. The setpoint error is simply the difference between the room air temperature and the setpoint bands. However, since the present is more certain, the errors occurring in the future have less weight. An exponential decay term is applied to the error vector:

$$C_{\text{SP}} = \beta_{\text{SP}} \left\| \; e^{-\alpha t} \left[(T_{\text{Heat}} - T)^{+} + (T - T_{\text{Cool}})^{+} \right] \right\|_2 \tag{8}$$

Second, to reduce oscillatory behaviour of the HVAC system that may lead to premature failure of equipment, a rate of change (ROC) penalty is applied as per Hovgaard et al. (2013):

$$C_{\text{ROC,W}} = \beta_{\text{ROC,W}} \left\| T_{\text{W}}^{t+1} - T_{\text{W}}^{t} \right\|_2, \quad t \in [0, T-1] \tag{9}$$

$$C_{\text{ROC,A}} = \beta_{\text{ROC,A}} \left\| T_{\text{A}}^{t+1} - T_{\text{A}}^{t} \right\|_2, \quad t \in [0, T-1] \tag{10}$$

The weights for the previous equations were chosen through a heuristic search.

Third, in Quebec, most commercial buildings fall under the Hydro-Quebec – provincial utility – Rate M (Hydro-Quebec, 2016). Unlike most providers in other localities that impose a time-of-use energy price, in Quebec, customers pay for their peak power and are therefore incentivized to have a flatter power demand. The following costs implement partially Rate M into the cost function:

$$C_{\text{PH,A}} = \$/kW \cdot \max(\dot{Q}_{\text{A}}^{+}) \tag{11}$$

Fourth, the energy balance of the building is minimized, *i.e.* if cooling is required in one zone and

heating in the next, both zones should exchange heat before requiring to extract or reject heat with the environment. The following cost penalizes heat transfer with the environment represented here by Q:

$$C_{\mathrm{E}} = \frac{\$/kWh \cdot \Delta t}{3600} \sum_{t=0}^{T} |\dot{Q}| \tag{12}$$

The control horizon and prediction horizon are set to 1 and 8 hours, respectively. To reduce the dimensionality of the problem – and the search space – a heterogenous time sampling approach was used (Hovgaard et al., 2013). The first 2 hours are sampled every 15 minutes, the 2 hours following are sampled every 30 minutes and the remaining 4 hours are sampled hourly, which results in 16 points for the slab inlet water temperature and 16 per HVAC supply air temperature.

The optimization is solved using the sequential least squares programming (SLSQP) algorithm which was developed by Dieter Kraft and implemented in the Scipy Minimize package. (Kraft, 1988, 1994; Jones et al., 2014) The SLSQP algorithm accepts bounds and/or constraints and can be used on nonlinear problems. The optimization routine approximates the cost function as a least squares problem and updates/iterates until convergence. Alternatively, the L-BFGS-B algorithm can be used, also implemented in Scipy Minimize; in our case, the SLSQP algorithm converged faster.

All the thermal nodes in the model were initialized at $19°C$. The first day served as a warm-up period and is not shown in any of the results – the first day is also omitted from Figure 4. Looking at the results for the base scenario of a vinyl tile covered 75 mm concrete hydronic slab in Figure 5, we can observe that the setpoints are generally respected. Since the simulated days were clear and although the exterior temperature was frigid, cooling is required for the south zone. The extracted heat from the room would be transferred to adjacent zones requiring heating in winter. The slab water inlet temperature is mostly at around room temperature, although there are periods of cooling that begin in anticipation of the peak solar gains. The peak can be eased by varying the penalty factor α_{SP} for the setpoint violation cost.

Effect of Design on Control

Many factors in the design of a radiant slab system affect the performance of the system, *e.g.* concrete type (density, specific heat), slab thickness, pipe spacing, pipe depth, layout, circuits in parallel, floor coverings and colour, as well as the building orientation, location, occupancy, window size and if there are complementary air systems. An exhaustive catalogue of every permutation cannot be easily compiled. Here, we have considered 3 slab thicknesses {38, 75, 150} mm and 3 typical floor coverings {vinyl tile, laminated wood and fibrous padded carpet} (see Table 2 for their thermal conductances). The piping is always at the bottom of the slab. The cost function is unchanged. Generally, carpets and cork materials should be avoided, as well as lightweight concretes ($<$1925 kg/m^3) due to higher porosity resulting in a higher thermal resistance (Nall, 2013). Looking at the 2$^{\mathrm{nd}}$ subplot of Figure 8, during noon, the wood and carpet finishes cannot conduct the solar gains and therefore remit the heat towards the room air potentially resulting in overheating. The vinyl tiles are thin and offer virtually no thermal resistance: the solar gains are absorbed into the concrete, shown by negative values. No obvious trend can be observed for the unoccupied periods.

The ability to maintain comfort is the central theme. The slab with wood and carpet coverings resulted

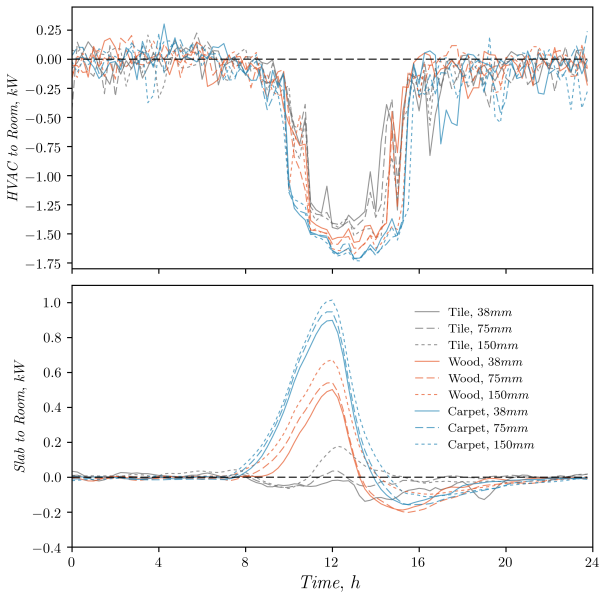

Figure 8: Heat transfer to the south zone room air node from the HVAC and slab surface. Showing middle day. Data mean-resampled on a 15-minute interval. Best viewed on a digital copy.

Table 1: Effect of air system cooling and heating peak demand for tile, wood and carpet finishes for the south and north zones for the simulated days.

		South		North	
	Slab	Cool	Heat	Cool	Heat
	mm	kW_{peak}			
Tile	38	-1.52	0.28	-2.05	0.96
	75	-1.55	0.29	-2.00	0.96
	150	-1.62	0.23	-1.93	0.69
Wood	38	-1.65	0.27	-2.32	1.00
	75	-1.65	0.36	-2.18	1.11
	150	-1.72	0.20	-3.12	1.13
Carpet	38	-1.80	0.36	-2.60	1.21
	75	-1.81	0.31	-2.02	0.73
	150	-1.82	0.30	-2.62	1.18

in more periods of overheating and even attaining temperatures above $29°C$ (see Figures 6 & 7 for histograms showing the number of minutes when the setpoint was violated for all cases). Looking at the peak air-side heating and cooling power (see Table 1), the heating power is similar for all cases since the radiant slab does not participate in the morning warm-up period; the optimization favours the slab to be used in cooling. It is possible that for cloudy days, the slab would be more utilized in heating; a full year simulation would be required. The parameters used in the cost function can be modified to change the behaviour of the system. The added thermal resistance of a wood or carpet covering increases the cooling peak since the slab is unable to effectively absorb the peak solar gains. It can be seen in Figure 8 where the heat transferred into the room from the HVAC and slab surface are shown. In both zones, the HVAC system varies notably every 15 minutes; by penalizing the rate of change (increasing $\beta_{\mathrm{ROC,A}}$), the output can be smoothened to reduce excessive wear on the equipment. Finally, during the noon periods, the thermal gains of the south zone are transferred to the north, reducing the need to extract heat from the environment.

Conclusion

This paper presented a model and model-based predictive control (MPC) methodology applied on an archetype zone containing a hydronic radiant slab. The MPC scheme was able to maintain the room temperature within the setpoint bands for the cases using vinyl as floor covering. When using insulating materials like wood and carpet, the slab is unable to absorb the peak solar gains and the room overheats. Given the cost function and the selected weights, the optimization routine favoured the slab to be used for cooling and the air system for the morning start-up.

The work presented here serves as the groundwork for the future implementation of MPC in the Varennes Net-Zero library. However, certain limitations must be addressed: the convection and radiative coefficients should vary with temperature, variable or staged flow rates should be used for the pumps and fans, actual building occupancy must be modelled including behavioural uncertainties, and, both model and optimization parameters should be tuned continuously for the zones they serve. Finally, the optimization must consider all the energy transactions of the building as well as the electricity production of the library's 120 kW photovoltaic array. The methodology can be extended for other storage mediums.

Acknowledgement

This study is part of an ongoing research at Concordia University funded under a Natural Sciences and Engineering Research Council (NSERC) & Hydro-Quebec Industrial Research Chair held by Dr. Athienitis. We would like to thank Jocelyn Millette from Hydro-Québec LTE-Shawinigan for his valuable input. Vasken Dermardiros is supported by the NSERC Alexander Graham Bell Doctorate Scholarship, the Hydro-Quebec ENCS Entrance Scholarship and the Concordia Faculty of ENCS Graduate Scholarship.

Table 2: Simulation parameters.

Time		
Simulation timestep	1	min
Control horizon	1	hour
Prediction horizon	8	hours
Radiant slab		
k_{concrete}	1.731	W/mK
ρ_{concrete}	2240	kg/m^3
$c_{\mathrm{p,concrete}}$	840	J/kgK
ρ_{water}	1000	kg/m^3
$c_{\mathrm{p,water}}$	4200	J/kgK
u_{tile}	110	W/m^{2}K
$u_{\mathrm{wood,12.7mm}}$	6.3	W/m^{2}K
$u_{\mathrm{carpet,fibrous}}$	2.7	W/m^{2}K
$k_{\mathrm{pipe,PEX}}$	0.51	W/mK
Pipe spacing	250	mm
Pipe depth	38, 75, 150	mm
Pipe int. diam.	9.525	mm
Pipe ext. diam.	12.7	mm
Water velocity	2	m/s
Section length	32	m
# of sections	4	-
Area per section	4	m^2
$T_{\mathrm{W,min}}$	10	°C
$T_{\mathrm{W,max}}$	32	°C
Room		
$u_{\mathrm{envelope,south}}$	0.564	W/m^{2}K
$u_{\mathrm{envelope,north}}$	0.304	W/m^{2}K
$u_{\mathrm{air,effective}}$	9	W/m^{2}K
$C_{\mathrm{effective,south}}$	2521	kJ/K
$C_{\mathrm{effective,north}}$	8257	kJ/K
$T_{\mathrm{A,min}}$	12	°C
$T_{\mathrm{A,max}}$	35	°C
Air volume change	6	ACH
Cross-ventilation	2	ACH
Window-wall ratio$_{\mathrm{south}}$	80	%
Window-wall ratio$_{\mathrm{north}}$	10	%
Cost function		
α_{SP}	0.025	-
β_{SP}	10	-
$\beta_{\mathrm{ROC,A}}$	0.010	-
$\beta_{\mathrm{ROC,W}}$	0.005	-
$, peak	14.37	$/kW
$, energy	0.0493	$/kWh

Nomenclature

Table 3: Nomenclature.

Scripts	
i	nodal index, active
j	nodal index, neighbouring
k	nodal index, known source
n	slab section index
t	time index
T	final time index
W	water
A	air
PH	peak heating
E	energy
ROC	rate of change, slew rate
Variables	
A	area, m^2
C	thermal capacitance, J/K
c_p	specific heat, J/kgK
k	conductivity, W/mK
M	# thermal nodes with known T°
$\dot{m}$	mass flow rate, kg/s
N	# thermal nodes
$\dot{Q}$	heat flow, W
T	temperature, $°C$
U_{ij}	conductance between i & j, W/K

References

ASHRAE (2008). ASHRAE Vision 2020: Producing Net Zero Energy Buildings. Technical report.

Bucking, S., A. K. Athienitis, and R. Zmeureanu (2014). Multi-Objective Optimal Design of a Near Net Zero Energy Solar House. *ASHRAE Transactions 120*, 224.

Camacho, E. F. and C. Bordons (2007). *Model Predictive control*. Advanced Textbooks in Control and Signal Processing. London: Springer London.

Candanedo, J. and A. Athienitis (2011). Predictive control of radiant floor heating and solar-source heat pump operation in a solar house. *HVAC&R Research 17*(3), 235–256.

Candanedo, J., J. Salom, J. Widn, and A. Athienitis (2015). Load matching, grid interaction, and advanced control. In A. Athienitis and L. O'Brien (Eds.), *Modeling, Design, and Optimization of Net-Zero Energy Buildings*, pp. 207–240. Wilhelm Ernst and Sohn.

Candanedo, J. A., A. Allard, and A. K. Athienitis (2011). Predictive Control of Radiant Floor Heating and Transmitted Irradiance in a Room with High Solar Gains. *ASHRAE Transactions 117*(2).

Cengel, Y. A., A. J. Ghajar, and H. Ma (2011). *Heat and Mass Transfer: Fundamentals & Applications* (4th ed.). McGraw-Hill.

Chen, Y., A. K Athienitis, and K. Galal (2012). Thermal performance and charge control strategy of a ventilated concrete slab (VCS) with active cooling using outdoor air. *ASHRAE Transactions 118*, 556.

Coffey, B., F. Haghighat, E. Morofsky, and E. Kutrowski (2010). A software framework for model predictive control with GenOpt. *Energy and Buildings 42*(7), 1084–1092.

Dermardiros, V. (2015). Modelling and Experimental Evaluation of an Active Thermal Energy Storage System with Phase-Change Materials for Model-Based Control. Master's thesis, Concordia University.

EIA (2016). U.S. Energy Information Administration (EIA). Available: `https://www.eia.gov/consumption/`.

Energy.ca.gov (2016). Building Energy Efficiency Program - California Energy Comission. Available: `http://www.energy.ca.gov/title24/`.

Gunay, H. B., J. Bursill, B. Huchuk, W. O'Brien, and I. Beausoleil-Morrison (2014). Shortest-prediction-horizon model-based predictive control for individual offices. *Building and Environment 82*, 408–419.

Hovgaard, T. G., S. Boyd, L. F. Larsen, and J. B. Jrgensen (2013). Nonconvex model predictive control for commercial refrigeration. *International Journal of Control 86*(8), 1349–1366.

Hydro-Quebec (2016). Hydro-Quebec Rates for Business Customers: Rate M. Available: `http://www.hydroquebec.com/business/rates-and-billing/rates/electricity-rates-business-customers/rate-m/`.

Jones, E., T. Oliphant, and P. Peterson (2014). SciPy: Open source scientific tools for Python.

Kraft, D. (1988). A software package for sequential quadratic programming. Technical report, DFVLR Obersfaffeuhofen, Germany.

Kraft, D. (1994). Algorithm 733: TOMPFortran modules for optimal control calculations. *ACM Transactions on Mathematical Software (TOMS) 20*(3), 262–281.

Lee, J. H. (2011). Model predictive control: Review of the three decades of development. *International Journal of Control, Automation and Systems 9*(3), 415–424.

May-Ostendorp, P., G. P. Henze, C. D. Corbin, B. Rajagopalan, and C. Felsmann (2011). Model-predictive control of mixed-mode buildings with rule extraction. *Building and Environment 46*(2), 428–437.

McSheffrey, E. (2016). Canada officially ratifies historic Paris climate agreement. Available: http://bit.ly/2htcDVc.

Nall, D. (2013). Thermally Active Floors. *ASHRAE Journal*.

NBI (2013). High Performance Buildings Measured Performance and Key Performance Indicators. Technical report, New Buildings Institutes.

NBI (2016). Zero Net Energy. Available: http://newbuildings.org/hubs/zero-net-energy/.

NRCan (2015). National Energy Use Database (NEUD). Available: http://oee.nrcan.gc.ca/corporate/statistics/neud/dpa/home.cfm.

Oldewurtel, F., A. Parisio, C. N. Jones, D. Gyalistras, M. Gwerder, V. Stauch, B. Lehmann, and M. Morari (2012). Use of model predictive control and weather forecasts for energy efficient building climate control. *Energy and Buildings 45*, 15–27.

Oldewurtel, F., A. Parisio, C. N. Jones, M. Morari, D. Gyalistras, M. Gwerder, V. Stauch, B. Lehmann, and K. Wirth (2010). Energy efficient building climate control using stochastic model predictive control and weather predictions. In *American control conference (ACC), 2010*, pp. 5100–5105. IEEE.

Olesen, B. W. (2008). Radiant Floor Cooling Systems. *ASHRAE Journal*.

Qin, S. J. and T. A. Badgwell (2003). A survey of industrial model predictive control technology. *Control engineering practice 11*(7), 733–764.

SNEBRN (2016). NSERC smart net-zero energy buildings strategic research network. Available: http://www.solarbuildings.ca.

Wang, S. and Z. Ma (2008). Supervisory and Optimal Control of Building HVAC Systems: A Review. *HVAC&R Research 14*(1), 3–32.